Directed flow of ϕ-mesons from Beam Energy Scan Au+Au collisions using the STAR detector
(Analysis Note)

Subhash Singha, Kent State University, Ohio, USA
(subhash@rcf.rhic.bnl.gov)
PA's of the Paper:
Olga Evdokimov, Declan Keane, Yadav Pandit, Prashanth Shanmuganathan, Subhash Singha, Gang Wang, Nu Xu
(Dated: November 22, 2016)

We will report the results of v_1 and dv_1/dy near mid-rapidity for ϕ-meson in Au+Au collisions at $\sqrt{s_{NN}}$ = 7.7, 11.5, 14.5, 19.6. 27, 39, 62.4 and 200 GeV. The dv_1/dy of Λ is found to be consistent with that of protons and shows a change in sign for $\sqrt{s_{NN}} < 14.5$ GeV. The v_1-slope for $\bar{\Lambda}$, $\bar{p}$ and ϕ shows similar trend for $\sqrt{s_{NN}} > 14.5$ GeV, while below 14.5 GeV ϕ v_1 is consistent with zero but with a large uncertainty. The dv_1/dy for net-proton and net-kaon is similar for $\sqrt{s_{NN}} > 14.5$ GeV, but they deviate at lower beam energies.

I. INTRODUCTION:

A goal of ultra-relativistic heavy-ion collisions at the Relativistic Heavy Ion Collider (RHIC) is to study the QCD phase diagram. STAR has taken data in the Beam Energy Scan (BES) program in order to extend measurements into new regions where the baryon density is high. The beam energy dependence of the slope of directed flow (dv_1/dy) for protons and net protons near mid-rapidity points to a possible softening of the equation of state. New v_1 measurements with different hadron species, having different constituent quarks, will help in disentangling the role of produced and transported quarks in heavy-ion collisions. In particular ϕ offers a unique advantage because of it's mass similar to proton but it is a vector meson. Due to small hadronic interaction cross sections, the ϕ-meson can be used as a clean probe to study the early dynamics. Moreover the v_1 measurements can also be used to test transport model calculations.

II. DATA SETS:

We have used the data collected in Beam Energy Scan Program at RHIC using the STAR detector. The analysis is done using the minimum bias data from Au+Au collisions at $\sqrt{s_{NN}}$ = 7.7, 11.5, 14.5, 19.6, 27, 39 , 62.4 and 200 GeV. The trigger Id and production Id for each beam energy used in this analysis is given in Table I.

$\sqrt{s_{NN}}$ (GeV)	Production Id	$\lvert v_Z\rvert(cm)$	$\lvert v_r\rvert(cm)$	BBC ADC Sum	Trigger Id	$N_{events} \times 10^6$
7.7	P10ih	< 70	< 2	15	290001, 290004	4
11.5	P10ih	< 50	< 2	15	310004, 310014	12
14.5	P10ih	< 50	< 1	75	440005, 440015	18
19.6	P11id	< 50	< 2	15	340001, 340011, 340021	36
27	P11id	< 50	< 2	75	360001, 360002	70
39	P10ik	< 40	< 2	75	280001, 280002	130
62.4	P10ik	< 30	< 2	–	270001, 270011, 270021, 280001	20
200	P11id	< 30	< 2	–	350003, 350013, 350023, 350033, 350043	200

TABLE I. Data Set, event cuts, triggers ids and number of event analyzed.

III. EVENT, TRACK AND PID SELECTION:

The good quality events are selected by applying a cut on the (X, Y) and Z-position of the collision vertex. These cuts remove beam gas backgrounds. The list of cuts on Z-position (v_Z) and r-position ($\sqrt{v_X^2 + v_Y^2}$) of the collision vertex for different beam energies are listed in Table I. The extreme right column in Table I gives the number of analyzed events after the event selection.

The good quality tracks are selected by applying the following cuts:

1. $0.15 < p_T < 10\ GeV/c$
2. -1.0 $< \eta <$ 1.0
3. Number of hits in TPC >= 15.
4. Number of hits in TPC/ Maximum number of hits in TPC> 0.52
5. $|DCA| < 3$ cm
6. Pair rapidity : $< |1.0|$

The ϕ meson is reconstructed via its hadronic decay to kaons. ($\phi \rightarrow K^+K^-$). Kaon tracks are identified utilizing the Time Projection Chamber (TPC) and Time of Flight (TOF) detectors. Particle identification in TPC is based on the specific energy loss (dE/dx) of each particle in the medium of the TPC. If TOF matched tracks are available we use the mass-square information to select kaons, otherwise we use specific energy loss in TPC. The PID selection scheme is following:

If the tracks are TOF-matched, we select tracks with TOF $\beta > 0$ and $0.16 < m^2 << 0.36$. Otherwise, we select tracks with $|N^{K^{\pm}}_{\sigma-TPC}| < 2$.

The specific energy loss of kaons in TPC as a function of momentum at beam energies 7.7 and 39 GeV are shown in the top panel of Figure 1. The bottom panel shows the TOF mass-squared distribution as a function of momentum at the same energies.

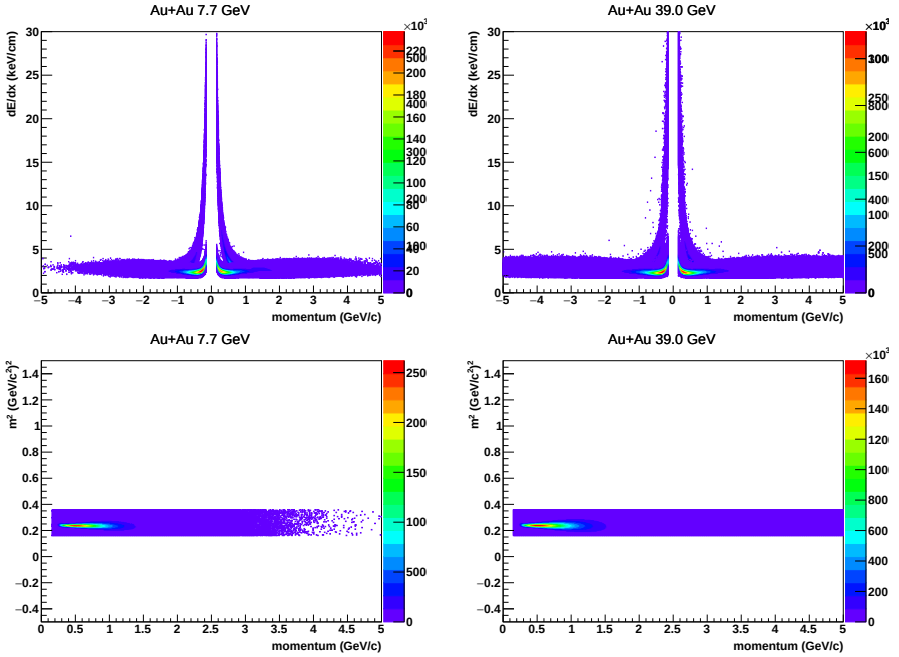

FIG. 1. Top panels: specific energy loss in TPC ($< dE/dx >$) as a function of momentum for $\sqrt{s_{NN}}$ = 7.7 and 39 GeV. Bottom panels: TOF mass-squared as a function of momentum for the same beam energies.

In order to get a good quality of the data, a bad run list for all beam energies (7.7 - 200 GeV) were prepared in StRefMultCorr class. These bad runs are removed from the analysis.
http://www.star.bnl.gov/cgi-bin/protected/cvsweb.cgi/offline/users/hmasui/

IV. ANALYSIS METHOD:

In this analysis event plane is reconstructed using the forward detectors, because the signal of v_1 is significant at forward rapidity rapidity region. Moreover a large η-gap between TPC and forward detectors reduces non-flow contribution. For the estimation of event plane angle, we use the Beam Beam Counter (BBC) for energies $\sqrt{s_{NN}}$ = 7.7 - 39 GeV, while at higher energies ($\sqrt{s_{NN}}$ ¿ 39 GeV) the BBC resolution is not good. So, we utilize the Zero Degree Caloremeters with a Shower Max Detector (ZDC-SMD) to estimate the event plane for beam energies, $\sqrt{s_{NN}}$ = 62.4 and 200 GeV. The methods used to reconstruct the event plane is discussed below.

A. Event plane reconstruction:

The reaction plane is defined as the plane spanned by the impact parameter and beam direction. But in real experiment the reaction plane information is not known because it is not possible to measure the impact parameter. So an estimate of reaction plane, called an event plane, is calculated using the flow itself. To estimate the event plane using BBC, we construct flow vectors,

$$Q_{nx} = \sum_i w_i cos(n\varphi_i) \tag{1}$$

$$Q_{ny} = \sum_i w_i sin(n\varphi_i) \tag{2}$$

Where φ_i is the fixed azimuthal angle of the BBC tiles. and w_i is the weight, defined as

$$w_i = \frac{ADC_i}{\sum_{i=1}^{i=16} ADC_i} \tag{3}$$

For the estimation of BBC event-plane we use only 16 inner tiles of BBC.

$$\Psi_n = \frac{1}{n}\, arctan(\frac{\sum_i w_i sin(n\varphi_i)}{\sum_i w_i cos(n\varphi_i)}) \tag{4}$$

Because of detector inefficiency and acceptance effects the event plane distribution is not flat, even if it is weighted by ADC. To make it flat, a further shifting method is applied. It makes the correction to the event plane itself, to get the flat event plane distribution.

$$n\Psi'_n = n\Psi + n\Delta\Psi \tag{5}$$

$$\Delta\Psi = \sum_{i=1}^{i=i_{max}} (A_i cos(in\Psi) + B_i sin(in\Psi)) \tag{6}$$

$$n\Psi'_n = n\Psi + \sum_{i=1}^{i=i_{max}} \frac{2}{i}[- < sin(in\Psi) > cos(in\Psi) + < cos(in\Psi) > sin(in\Psi)] \tag{7}$$

The Figure 2 shows shift corrected first order event plane distribution obtained using the BBC as described above.

Due to the finite number of particles used to reconstruct the event plane, there is a finite resolution in the estimated event plane. Thus the estimated v_1 has to be corrected for the event plane resolution. The event plane resolution of the first order event plane resolution, is obtained by using the correlation between the east and west sector of the BBC. The Figure 3 shows the first order event plane resolution as a function of centrality for $\sqrt{s_{NN}}$ = 7.7 - 39 GeV.

From Figure 3, one can see that the first order event plane resolution using BBC become poor as one go from lower to higher beam energies. So for higher two beam energies in this analysis, namely $\sqrt{s_{NN}}$ = 62.4 and 200 GeV, we use ZDC-SMD detector to estimate the event plane. In this method we utilize the sideward deflection of spectator neutrons measured in the ZDC-SMD. For this purpose, we use 7 vertical slats and 8 horizontal slats of the ZDC-SMD. The two SMDs provide event-by-event information on the transverse distribution of energy deposition of the spectator neutrons. The weighted center of the energy distribution determines the event plane vector on each side. The combination of the east and west event plane vectors provides the full event plane. Measurements using ZDC-SMD is sensitive to the calibration. Since the transverse position of the beam is not stable, the centroid in ZDC-SMD varies time to time. This beam center calibration is done, before reconstructing the event plane. In addition the ADC distributions are pedestal subtracted and the gain corrected in order to make a uniform gain over all the detector. The flow vector's are constructed as following:

$$Q_{nx} = \sum_{i=1}^{7} w_i x_i \tag{8}$$

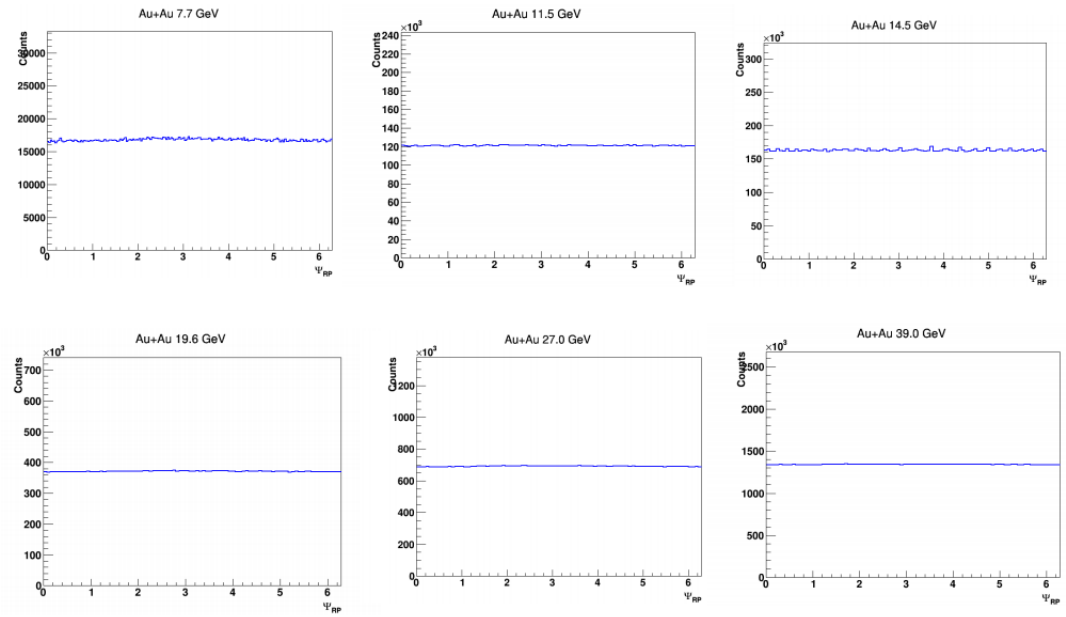

FIG. 2. First order full event plane (Ψ_1) distribution using BBC at $\sqrt{s_{NN}}$ = 7.7 - 39 GeV.

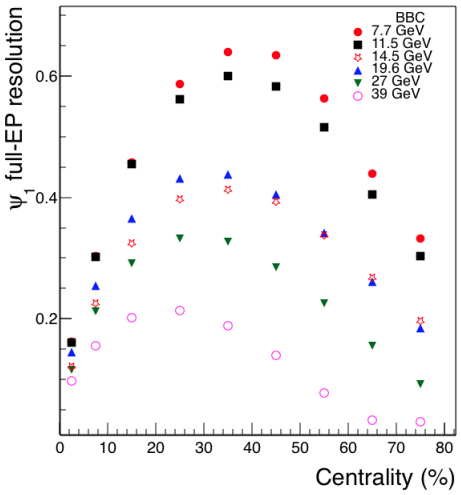

FIG. 3. First order full event plane (Ψ_1^{full}) resolution (using east and west BBC) as a function of collision centrality for $\sqrt{s_{NN}}$ = 7.7 - 39 GeV.

$$Q_{ny} = \sum_{i=1}^{8} w_i y_i \tag{9}$$

And the event plane angle is defined as,

$$\Psi_n = \ arctan(\frac{\sum_{i=1}^{7} w_i x_i}{\sum_{i=1}^{8} w_i y_i}) \tag{10}$$

Where x_i and y_i's are the fixed position for the 7 vertical slats and 8 horizontal slats in the ZDC-SMD. w_i is the weighted ADC defined as,

$$w_i = \frac{ADC_i}{\sum_{i=1}^{i=7or8} ADC_i} \tag{11}$$

Event plane should be randomly distributed, but because of the rectangular geometry of the ZDC-SMD the shape of the event plane distribution is not flat. The event plane distribution is flattened by using a shift method as described above for BBC. The left panel in Figure 4 shows the shift corrected ZDC-SMD event plane distribution for $\sqrt{s_{NN}}$ = 62.4 and 200 GeV. The event-plane resolution is obtained from the correlation of the two event plane vectors (east and west ZDC) in the similar way as discussed in the section above for BBC. The right panel in Figure 4 shows the first order ZDC-SMD event plane resolution for $\sqrt{s_{NN}}$ = 62.4 and 200 GeV. More details on the ZDC-SMD analysis can be found here:

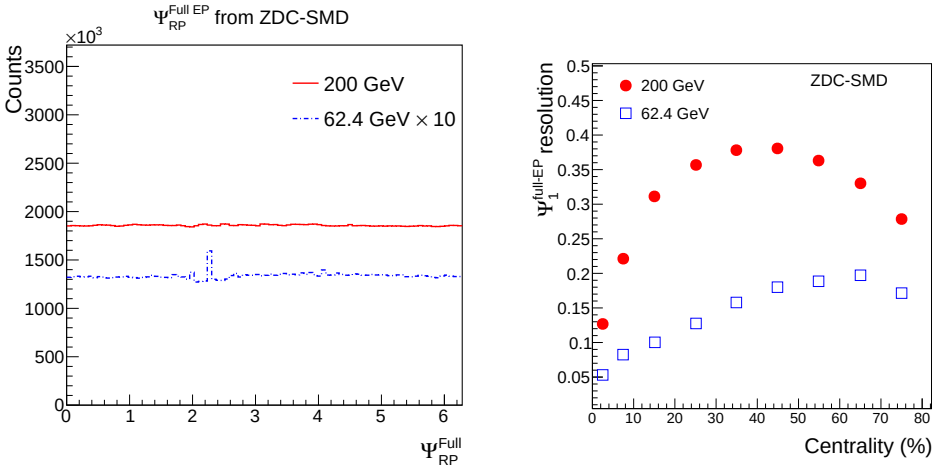

FIG. 4. Left panel: First order full event plane (Ψ_1) from ZDC-SMD for $\sqrt{s_{NN}}$ = 62.4 and 200 GeV. Right panel: First order ZDC full event plane (Ψ_1^{full}) resolution as function of collision centrality for $\sqrt{s_{NN}}$ = 62.4 and 200 GeV.

https://www.star.bnl.gov/protected/bulkcorr/subhash/presentations/work/phi_v1_62_ZDCSMD.pdf
https://www.star.bnl.gov/protected/bulkcorr/subhash/presentations/work/phi_v1_200_ZDCSMD.pdf

B. Signal reconstruction:

The ϕ-meson is reconstructed through it's hadronic decay channel ($\phi \rightarrow K^+K^-$). The charged kaons are selected using both the TPC and TOF detector as discussed in the previous section. The left panel in Figure 5 shows the same event K^+K^--invariant mass distribution for Au+Au collisions at $\sqrt{s_{NN}}$ = 19.6 GeV within the rapidity window $-1 < y < 1$. The ϕ-signal is observed on top of a residual background. The combinatorial background is constructed via mixed event method. In this method, K^+K^- pairs are taken from 5 events with similar v_Z and collision centrality. We considered 10 bins in v_Z and 10 bins in centrality percentile. The right panel in Figure 5 shows the K^+K^--invariant mass distribution after the combinatorial mixed event background subtraction. The signal is fitted with a Breit-Wigner function and a linear residual function,

The mass and width of ϕ-meson is extracted by fitting the invariant mass distribution with a Breit Wigner function as defined below:

$$\frac{Y}{2\pi}\frac{\Gamma_0}{(M(K\pi) - M_0)^2 + \frac{\Gamma_0^2}{4}} + (AM + B). \tag{12}$$

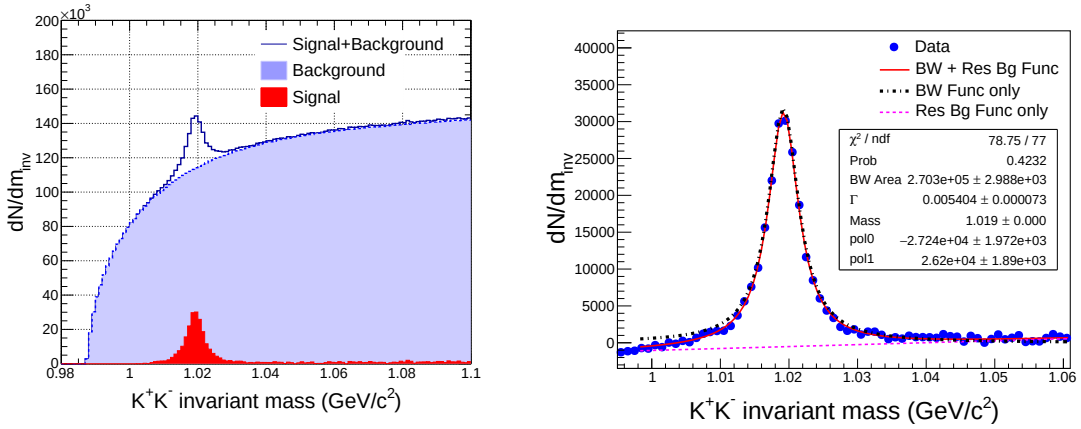

FIG. 5. Example of ϕ-meson invariant mass reconstruction using mixed event method.

Where M_0 and Γ_0 are the mass and width of ϕ-meson. Y denotes the area under the Breit-Wigner function. A and B are the coefficients of the linear residual background function. Using this above method the mass, width and yield of ϕ-meson is extracted in several rapidity bins (between $-1 < y < 1$) for $\sqrt{s_{NN}}$ = 7.7 - 200 GeV.

The top left and right panel of Figure 6 shows the mass and width of ϕ-meson as a function of rapidity extracted using Breit Wigner function for $\sqrt{s_{NN}}$ = 7.7 - 39 GeV. The uncertainties on the data point are only statistical. The mass peak position seems to be consistent with the standard PDG value but the results at 14.5 GeV shows different trend. Also the invariant mass width at 14.5 is larger than other beam energies. This could be a possible effect from Heavy Flavor Tracker (HFT) Detector installed during run 2014. The bottom panel in Figure 6 shows the signal-to-background ratio of ϕ-meson as a function of rapidity for $\sqrt{s_{NN}}$ = 7.7 - 39 GeV.

C. v_1 versus invariant mass method:

The ϕ-meson v_1 is extracted using invariant mass method. In this method first the combined v_1 (signal + background) is estimated as a function of invariant mass. Then we decompose $v_1^{Sig+Bg}(m_{inv})$ as,

$$v_1^{Sig+Bg}(m_{inv}) = \frac{Sig}{Sig+Bg} v_1^{Sig} + \frac{Bg}{Sig+Bg} v_1^{Bg} \tag{13}$$

Where "Sig" is the signal yield and "Bg" is the background yields. The term v_1^{Bg} is parameterized by a second order polynomial of invariant mass. The v_1^{Sig} is estimated from fitting which is corrected for event plane resolution on event-by-event basis.

Examples of such extraction of ϕ-meson v_1 for 10−40% Au+Au collisions at $\sqrt{s_{NN}}$ = 19.6, 39 and 200 GeV are shown in Figure 7. The solid black lines are the total $v_1^{Sig+Bg}(m_{inv})$, while the signal ($\frac{Sig}{Sig+Bg} v_1^{Sig}$) and background ($\frac{Bg}{Sig+Bg} v_1^{Bg}$) components are shown by dotted blue and red lines. The v_1 for ϕ-meson as a function of rapidity is extracted using this method for $\sqrt{s_{NN}}$= 7.7-200 GeV. The v_1-slopes are extracted by a linear fit to the data. The statistical uncertainties in the measurements of ϕ v_1 at 7.7 and 62.4 GeV are too large and hence it is not feasible to extract the slope at these two beam energies.

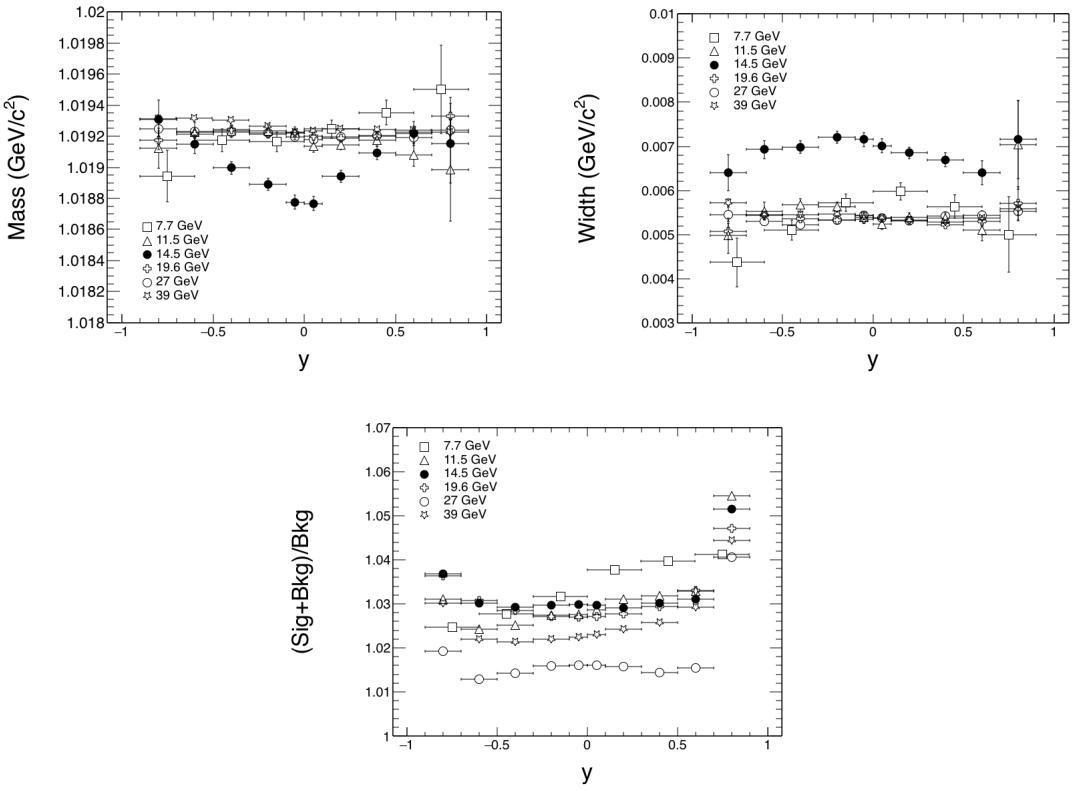

FIG. 6. Mass peak position (Top left panel), width (Top right panel) and signal to background ratio (Bottom panel) of ϕ-meson as a function rapidity in Au+Au collisions at $\sqrt{s_{NN}}$ = 7.7 - 39 GeV.

V. RESULTS:

The Figure 8 shows the v_1 as a function of rapidity for 0-10%, 10-40% and 40-80% centralities for $\sqrt{s_{NN}}$ = 7.7 - 200 GeV. The slope of v_1 at mid-rapidity (dv_1/dy) is extracted by fitting the v_1 vs y data to a straight line ($p_0 \times x$) passing through the (0, 0).

A. Systematic uncertainties

To study systematic uncertainty on the v_1-slope, the following cuts are varied:
— vary v_Z cut
— vary number of hits in TPC
— vary number possible hits/number of maximum hit in TPC
— vary DCA distribution
— vary TPC $n\sigma$ cuts
— vary fitting ranges for v_1 vs. y
— vary fitting ranges in invariant mass distribution
— different yield extraction (bin counting vs functional integration)
— effect of detector acceptance × efficiency

Details of the systematic study is shown in the following link: https://www.star.bnl.gov/protected/bulkcorr/subhash/presentations/work/status_phi_v1_26Oct_2015.pdf

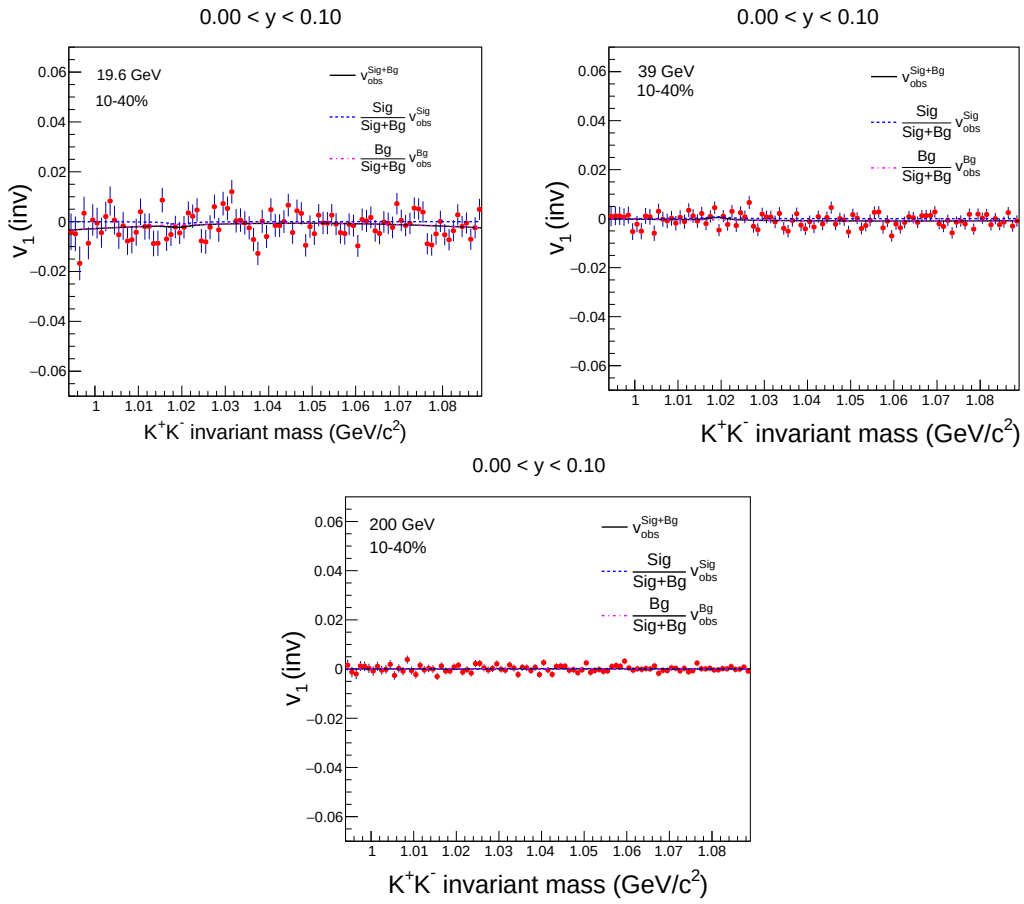

FIG. 7. Examples of ϕ-meson v_1 extraction through K^+K^- invariant mass for Au+Au collisions at $\sqrt{s_{NN}}$ = 19.6, 39 and 200 GeV.

B. slope of v_1

The left panel in Figure 9 shows the dv_1^{ϕ}/dy vs $\sqrt{s_{NN}}$ for 10-40 % centrality. The ϕ v_1 slope is compared to the λ, $\bar{\Lambda}$ and $K^{\pm}$. It is observed that for $\sqrt{s_{NN}}$ >= 14.5 GeV the ϕ v_1-slope is comparable to that of $\bar{\Lambda}$ while it is zero (with a large uncertainty) for $\sqrt{s_{NN}}$=11.5 GeV. It is observed that the beam energy dependence of dv_1/dy of $\bar{\Lambda}$ is consistent with the trend of anti-protons [8]. This indicates that the particles with produced constituent quarks exhibit similar flow.

These results of dv_1/dy is also compared with the expectations from UrQMD model (version 3.p2). The Figure 9 shows the comparison of dv_1/dy for λ, $\bar{\Lambda}$, $K^{\pm}$ and ϕ-meson with the UrQMD model calculations (shown by shaded bands). Although the UrQMD explains the data qualitatively at higher energies, it fails to reproduced the data at lower energies.

VI. SUMMARY:

We have presented v_1 and dv_1/dy near mid-rapidity for ϕ-meson in Au+Au collisions at $\sqrt{s_{NN}}$ = 7.7, 11.5, 14.5, 19.6. 27, 39, 62.4 and 200 GeV. The $dv_1/dy$of ϕ meson show similar trends as anti-proton and anti-Λ's. Lower energy data requires more statistics for a clear interpretation of v_1-slope. BES-II with more

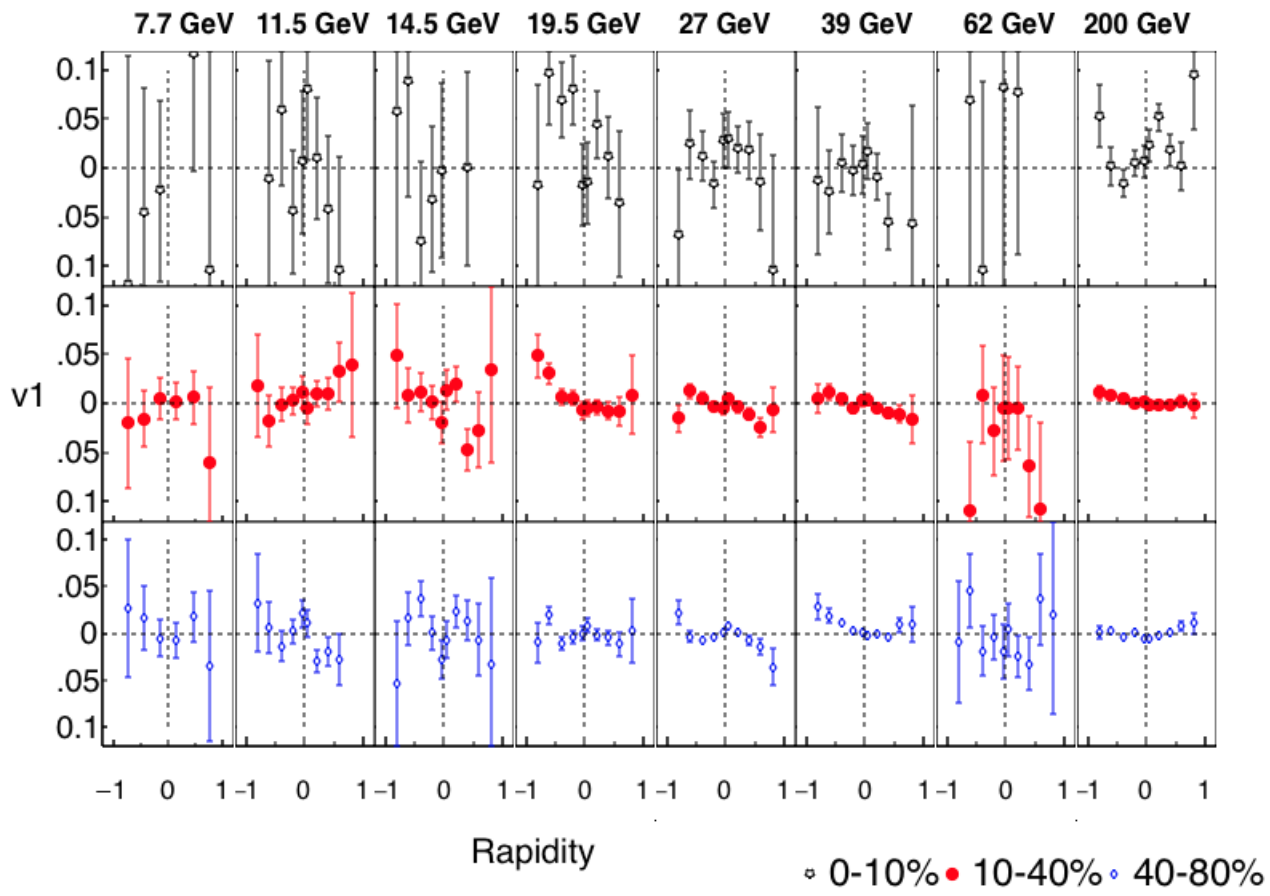

FIG. 8. ϕ-meson v_1 as a function rapidity for three different centrality intervals in Au+Au collisions at $\sqrt{s_{NN}}$ = 7.7 - 200 GeV.

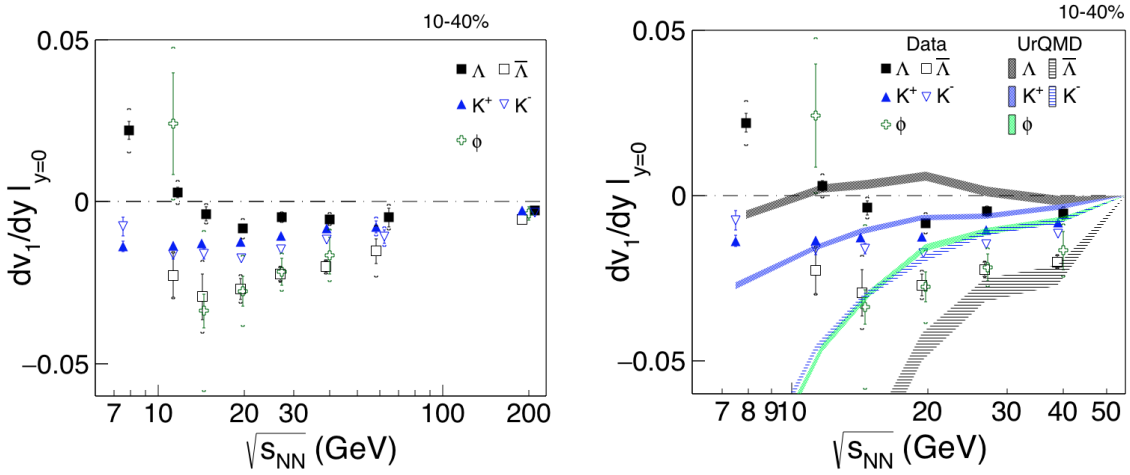

FIG. 9. Left panel: Comparison of dv_1/dy of ϕ-meson with *Lambda*, $\bar{\Lambda}$, $K^{\pm}$ for Au+Au collisions at $\sqrt{s_{NN}}$ = 7.7 - 200 GeV. Right panel: Comparison of the data in the left panel with UrQMD model calculations.

statistics and upgraded detectors will significantly improve the ϕ v_1-measurements.

[1] STAR ZDC-SMD proposal, STAR Note SN-0448 (2003).
[2] G. Wang, PhD thesis, Kent State University, 2005; https://drupal.star.bnl.gov/STAR/theses.
[3] The STAR ZDC-SMD has the same structure as the STAR EEMC SMD: C. E. Allgower *et al.*, Nucl. Instr. Meth. A **499**, 740 (2003).
[4] Y. Pandit, PhD thesis, Kent State University, XXXX; https://drupal.star.bnl.gov/STAR/theses.
[5] L. Adamczyk *et al.* (STAR Collaboration), Phys. Rev. Lett. **112**, 162301 (2014).
[6] S. A. Bass et al., Prog. Part. Nucl. Phys. **41**, 255 (1998).
[7] M. Bleicher, E. Zabrodin, C. Spieles, S. A. Bass, C. Ernst, S. Soff, L. Bravina, M. Belkacem, H. Weber, H. Stöcker and W. Greiner, J. Phys. G **25**, 1859 (1999).
[8] P. Shanmuganathan, PhD thesis, Kent State University, XXXX; https://drupal.star.bnl.gov/STAR/theses.

VII. LINK TO BULKCORR PRESENTATIONS:

https://www.star.bnl.gov/protected/bulkcorr/subhash/presentations/bulkcorr/phi_v1_BES_bulkcorr_20141210.pdf
https://www.star.bnl.gov/protected/bulkcorr/subhash/presentations/bulkcorr/phi_v1_BES_bulkcorr_20150225.pdf
https://www.star.bnl.gov/protected/bulkcorr/subhash/presentations/bulkcorr/status_phi_v1_BES_20150429.pdf
https://www.star.bnl.gov/protected/bulkcorr/subhash/presentations/bulkcorr/status_phi_v1_20151104.pdf
https://www.star.bnl.gov/protected/bulkcorr/subhash/presentations/bulkcorr/directed_flow_bes_sqm16_ver2.pdf

VIII. SQM PRESENTATION:

https://www.star.bnl.gov/protected/bulkcorr/subhash/sqm2016/
https://www.star.bnl.gov/protected/bulkcorr/subhash/sqm2016/proc/

IX. INT-16-3 PRESENTATION:

http://www.int.washington.edu/talks/WorkShops/int_16_3/People/Singha_S/Singha.pdf

X. ANALYSIS SOFTWARE:

https:https://www.star.bnl.gov/protected/bulkcorr/subhash/phiv1_docu/code_phiv1/

XI. APPENDIX:

A. QA plots:

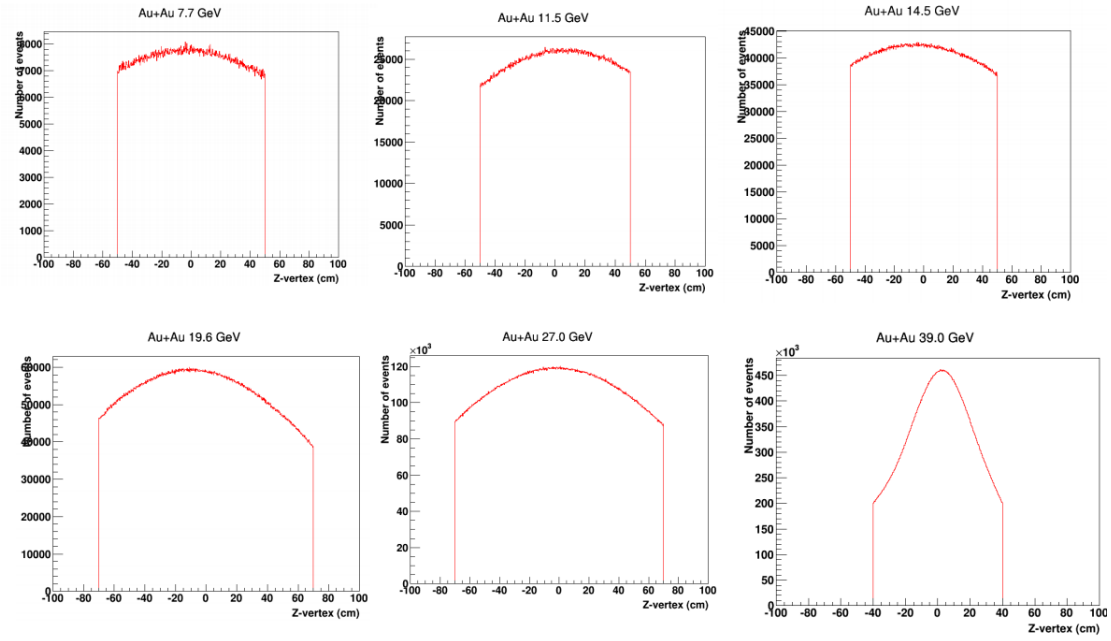

FIG. 10. z-position of vertex distribution for Au+Au collisions at $\sqrt{s_{NN}}$ = 7.7 - 39 GeV.

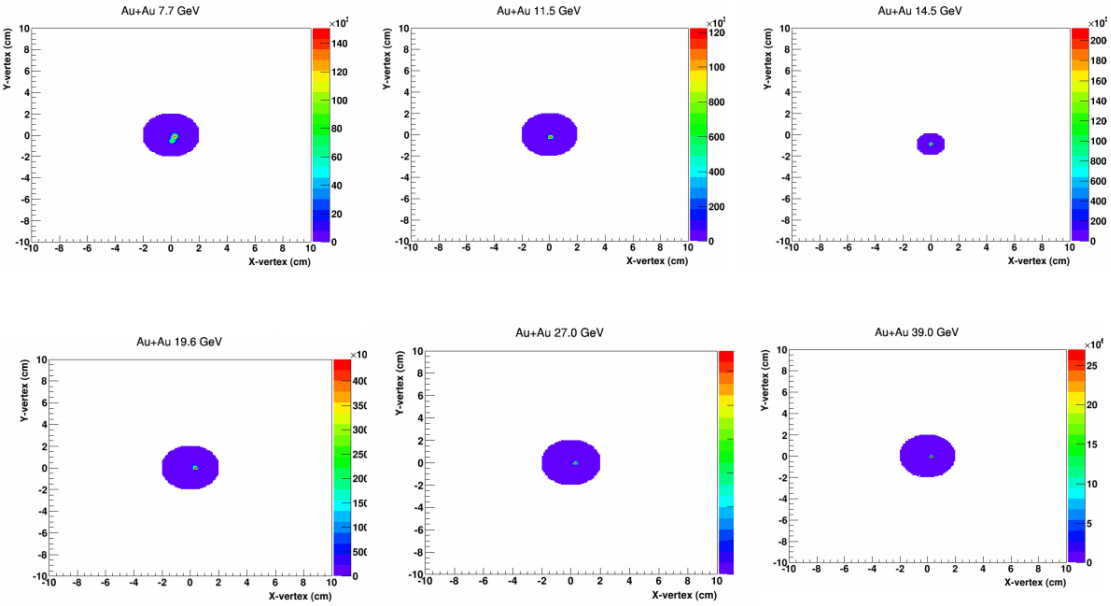

FIG. 11. x-y position of vertex for Au+Au collisions at $\sqrt{s_{NN}}$ = 7.7 - 39 GeV.

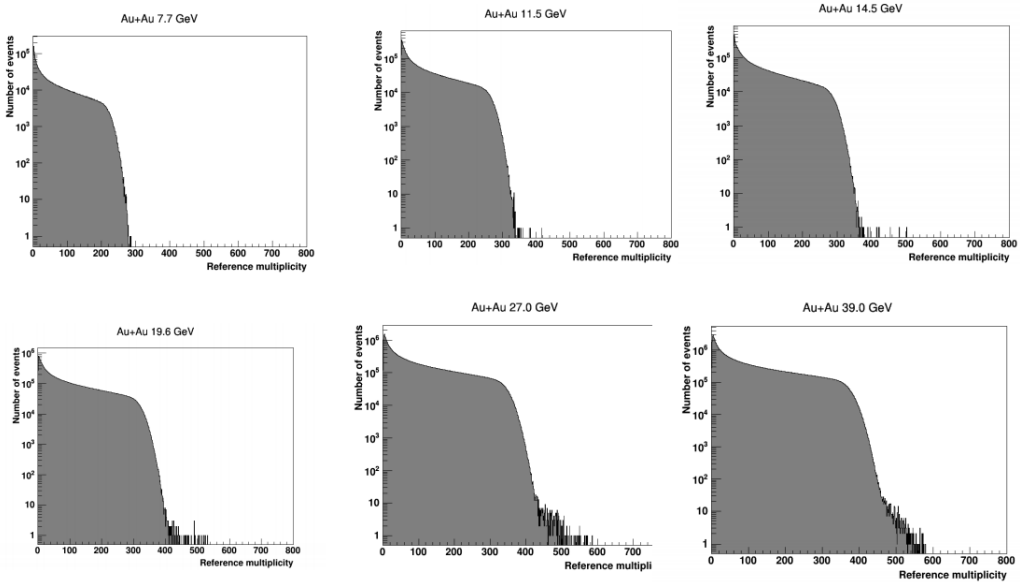

FIG. 12. reference multiplicity distribution for Au+Au collisions at $\sqrt{s_{NN}}$ = 7.7 - 39 GeV.